American Mineralogist, Volume 73, pages 1449–1456, 1988

Sputter depth profiling in mineral-surface analysis

MICHAEL F. HOCHELLA, JR.
Department of Geology and Center for Materials Research, Stanford University, Stanford, California 94305, U.S.A.
JAMES R. LINDSAY, VICTOR G. MOSSOTTI
U.S. Geological Survey, 345 Middlefield Road, M.S. 938, Menlo Park, California 94025, U.S.A.
CARRICK M. EGGLESTON
Department of Applied Earth Sciences, Stanford University, Stanford, California 94305, U.S.A.

ABSTRACT

The effects of ion bombardment on homogeneous samples of quartz, albite, calcite, and anhydrite have been studied with X-ray photoelectron spectroscopy (XPS) in order to better understand the usefulness and limitations of sputter depth profiles of minerals. Under the experimental conditions used (45° incident 1-kV Ar ions for a total of 20 min per sample; total ion dose = 10^{17} ions/cm^2), between 10 and 20 nm have been sputtered from each sample. XPS measurements have shown that compositional and structural modifications occur in the upper few nanometers of the mineral surface within the first minute of sputtering and after less than 1 nm of surface removal. The extent of the ion-induced modifications in the near-surface region reaches an apparent near-steady state after 3 to 4 min of sputtering. Therefore, after this time, significant changes in atomic concentrations as measured by XPS or Auger electron spectroscopy (AES) should indicate a true compositional gradient inherent to an unknown sample and not to the sputtering process itself. In addition, a sputter profile from a standard homogeneous sample similar to an unknown can provide a basis for interpreting the entire unknown profile despite preferential sputtering. Unfortunately, preferential sputtering and structural modifications preclude useful interpretations of oxidation state and atomic structure information from the photoelectron spectra during depth profiling. In addition, although the use of implanted Ar as a charge-reference standard is theoretically sound, we have found that the structural damage to mineral near-surfaces during even light implantations is significant; thus, the usefulness of this method of charge referencing for minerals is greatly diminished.

INTRODUCTION

The chemical analysis of mineral surfaces via X-ray photoelectron and Auger electron spectroscopies (XPS and AES, respectively) has been vital in advancing our understanding of important fundamental geochemical processes such as mineral dissolution and weathering (e.g., Petrovic et al., 1976; Thomassin et al., 1977; Berner and Holdren, 1977, 1979; Holdren and Berner, 1979; Fung et al., 1980; Schott et al., 1981; Perry et al., 1983) and sorption reactions at the water-mineral interface (e.g., Bancroft et al., 1977; Murray and Dillard, 1979; Brule et al., 1980; Dillard et al., 1982; Perry et al., 1984; Mucci et al., 1985; Mucci and Morse, 1985). New applications of these and other surface-sensitive techniques to geochemical studies should continue to expand this field of research (e.g., Petit et al., 1987; Hayes et al., 1987; Myhra et al., 1988; Hochella et al., 1986a, 1986b, 1988; Hochella and Brown, 1988).

Ion bombardment of surfaces is often used in conjunction with XPS and AES to obtain compositional information as a function of depth (in the geochemical literature, e.g., Perry et al., 1983; Mucci et al., 1985; White and Yee, 1985; Hochella, 1988). The need and usefulness of the combination of XPS-AES and ion bombardment become apparent when the surface sensitivities of XPS and AES are considered. For silicate mineral surface analysis, characteristic photo- and Auger electrons generally come from no deeper than approximately 1 to 10 nm depending on their energy. These depths of analyses can be determined by experiment (e.g., Hochella and Carim, 1988) or from theoretical calculations (e.g., Seah and Dench, 1979; Powell, 1984; Penn, 1987). Compositional profiling as a function of depth can be performed nondestructively within the depth of analysis using angle-resolved XPS or AES (this is done by limiting the collection of electrons to narrow angular ranges with respect to the surface). However, if compositional information is needed deeper than this, ion bombardment is necessary to sputter (erode) into the solid followed by additional XPS and/or AES analyses. This combination of ion bombardment and surface analysis, commonly called *sputter depth profiling,* can be used to obtain compositional information between the near-surface (to a depth of several nanometers) and the bulk as typically determined, for example, with the electron microprobe.

0003–004X/88/1112–1449$02.00

Ion bombardment has also recently been used to implant small amounts of Ar into insulating materials for use as a charge-reference standard for absolute binding energy measurements (Kohiki et al., 1983a, 1983b). This technique is potentially important for a more precise evaluation of oxidation and structural-state information from XPS spectra of minerals.

Considering the present and future importance of ion bombardment in the study of minerals, it is essential to understand all of the effects that energetic bombarding ions have on surfaces. Noble gases, accelerated to between 0.5 and 5.0 kV, are commonly used for sputtering, and their penetration into solids can be up to several tens of nanometers at the upper end of this energy range, depending on the bombarding ion, the target material, channeling effects, the angle of incidence, and so on (e.g., see Carter and Colligon, 1968; Howitt, 1986). A bombarding ion can be scattered back into the vacuum after interaction with the target, or it may remain implanted in the target. Physical sputtering occurs when target atoms or atom clusters are ejected into the vacuum, typically with a neutral charge, after interaction with the bombarding ion or other excited species from the target itself. However, sputtering processes tend to be inefficient, and much of the energy of the incident ion, on the average, is converted into target heating. Besides sputtering, heating, and implantation processes, ion bombardment can also result in the typically unwanted alteration of the near-surface composition (irrespective of the implantation) and atomic structure (e.g., see the general review by Hofmann, 1980). If these effects are not taken into account, gross misinterpretation of sputter depth profiles can easily be made.

Compositional and structural modifications of near-surfaces resulting from ion bombardment have been studied extensively and systematically for many classes of materials (Storp, 1985, and references therein). However, only a few studies have included minerals or materials with mineral compositions (Yin et al., 1972, 1976; Braun et al., 1977; Tsang et al., 1979; Coyle et al., 1981; Fischer et al., 1983), and a detailed and systematic study of mineral sputtering has never been made. The purpose of this paper is to briefly but systematically and carefully explore ion-induced compositional and structural modifications for several common minerals so that sputter depth profiles can be properly interpreted. In order to achieve this, XPS measurements have been performed both before and after various durations of Ar ion bombardment on an oxide, silicate, carbonate, and sulfate (quartz, albite, calcite, and anhydrite, respectively). Although we have performed sputtering experiments on many other minerals, these four are fairly representative of the effects of ion bombardment on mineral near-surfaces.

Experimental details

Single crystals of quartz (Herkimer County, New York), albite (Amelia, Virginia), calcite (location unknown), and anhydrite (Morningstar, Nevada) were chosen for surface analysis. Individual specimens were selected for their apparent purity and lack of visible inclusions. After degreasing in acetone and ethanol, each crystal was broken in air just before introduction into the surface-analytic instrument. XPS analysis and ion bombardment were conducted only on surfaces exposed by fracture. The analytic areas were either perfect cleavage surfaces (for albite, calcite, and anhydrite) or very smooth conchoidally fractured surfaces (for quartz).

All XPS spectra were collected on a VG ESCALAB MK II system. Instrument vacuum was in the 10^{-10} torr range. Nonmonochromatic Al X-rays were used with an analyzer pass energy of 50 eV (survey scans) and 20 eV (high-resolution scans). Surface-charge neutralization with an electron flood gun was not necessary. Charge corrections for each specimen were made by referencing to known energies of the following lines: quartz O 1*s*, 532.9 eV (Hochella and Brown, 1988); albite O 1*s*, 531.0 eV (Hochella and Brown, 1988); calcite O 1*s*, 531.9 eV (Wagner et al., 1979); and anhydrite S 2*p*, 168.5 eV (Lindberg et al., 1970).

For each sample, XPS spectra were collected from the freshly fractured surface and then after 1, 3, 6, 10, and 20 min of sputtering (i.e., the total sputtering time for each sample was 20 min). Ion bombardment was performed with 1-kV Ar ions. Ion current densities of approximately 10 $\mu A/cm^2$ were used resulting in total ion doses of 10^{17} ions/cm^2 after 20 min of sputtering. The angle of incidence for the ions with respect to the mineral surface was approximately 45°. Under these conditions, the ion gun used has been calibrated to sputter amorphous SiO_2 at the rate of 0.7 nm/min. Although the same sputtering conditions were used throughout this study, the actual sputtering rates for each specimen also depends on the mineral composition, its atomic structure, and the crystallographic orientation of the sample with respect to the ion beam. Considering these factors and judging from the tabulation of sputtering yields for a variety of materials as presented in Carter and Colligon (1968), we have estimated that the sputtering rate for any of the minerals used in this study under constant beam conditions should not vary by more than a factor of two, and it is likely that the actual sputtering rates will vary by much less than this. Therefore, it is most likely that all four samples in this study have had somewhere between 10 and 20 nm of surface removed after 20 min of sputtering.

Results

The changes in the photoelectron peak-intensity ratios (designated Δ%) as a function of sputtering time for quartz, albite, calcite, and anhydrite are shown in Figure 1. The change in these intensity ratios is directly proportional to the change in the corresponding near-surface atomic ratios. Specifically, results from the quartz sputtering experiment are presented in Figures 1a and 2. After 1 min of sputtering, the O/Si atomic ratio is reduced by 11% and thereafter remains nearly constant to the end of the experiment. The widths, measured as full width at half maximum (FWHM), of the O 1*s* (Fig. 2) and Si 2*p* photoelectron peaks increase steadily over the duration of the experiment by an average of approximately 30%. Despite the increase in width, the peak shapes remain symmetrical.

Unlike quartz, the changes in the atomic ratios of the albite near-surface occur most rapidly in the first 3 to 4 min of sputtering before leveling off (Fig. 1b). The largest changes in Δ% for albite involve the Al/Si ratio, which

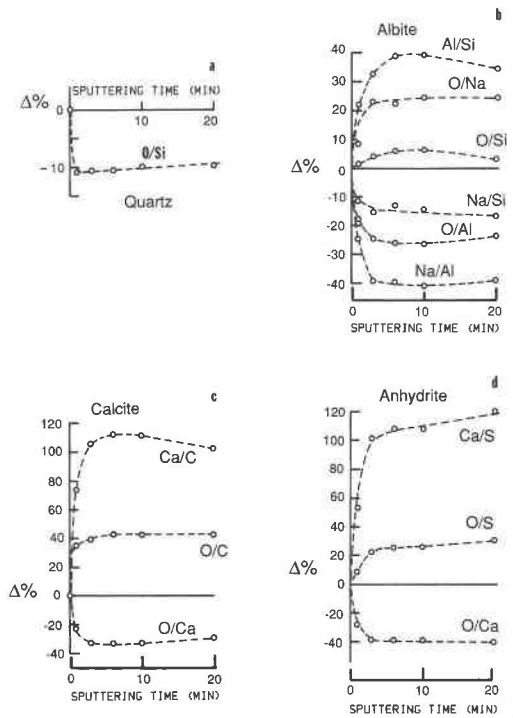

Fig. 1. Variation in atomic ratios, Δ% (percent change relative to the composition of the unsputtered surface), in the near-surface regions of (**a**) quartz, (**b**) albite, (**c**) calcite, and (**d**) anhydrite as a function of sputtering time as determined by XPS.

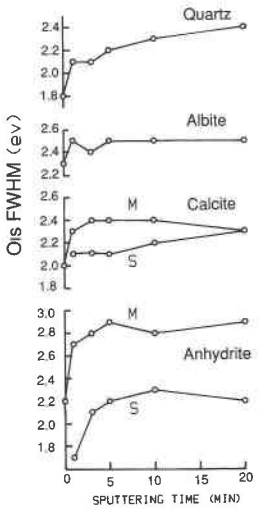

Fig. 2. O 1*s* photoelectron peak width, measured as full width at half maximum (FWHM), as a function of sputtering time for quartz, albite, calcite, and anhydrite. For quartz and albite, the O 1*s* peak simply broadens with increasing sputtering time. For calcite and anhydrite, however, sputtering not only broadens the original or main O 1*s* line (labeled M), but it creates a resolved or partially resolved shoulder (labeled S) that also broadens with sputtering time. The widths of the overlapping M and S O 1*s* components were determined by using a Gaussian-Lorentzian curve-fitting routine.

increases approximately 40% with respect to stoichiometry, and the Na/Al ratio, which decreases 40%. The widths of the O 1*s* (Fig. 2), Na *KLL*, Al 2*p*, and Si 2*p* peaks all increase with time of sputtering, although the form of the peak shapes, as with quartz, remain the same. The peak with the largest width increase (30%) after 20 min of sputtering is the Na *KLL* Auger line.

As a check for reproducibility, a second fresh albite surface was sputtered, this time for a total of 30 min. After 20 min of sputtering, the results were the same as shown in Figure 1b within the estimated error of Δ% (±10% relative). Between 4 and 30 min of sputtering, none of the ratio curves exhibit a positive or negative trend, and therefore each atomic ratio seems to have reached a steady-state value after only 4 min.

The results of the calcite sputtering experiment are shown in Figures 1c, 2, and 3. The O/C and Ca/C atomic ratios both increase after just 1 min of sputtering, the latter dramatically, whereas the O/Ca intensity ratio undergoes a substantial decrease (Fig. 1c). From 3 min of sputtering to the end of the experiment, all three ratios show little to no change. In addition, the Ca $2p_{3/2,1/2}$ spin-orbit split lines and the C 1*s* peak become wider with sputtering. On the other hand, sputtering generates a new clearly resolved O 1*s* line (Figs. 2 and 3).

The O/S, O/Ca, and Ca/S atomic ratios for anhydrite all show substantial changes during sputtering, particularly the latter ratio, which more than doubles after just 3 min of sputtering (Fig. 1d). In addition, as with the other samples in this study, all peaks broaden with time of sputtering (see Fig. 2 for the O 1*s* widths). The S 2*p* and O 1*s* lines also develop shoulders on their low-binding-energy sides. For example, Figure 4 shows the S 2*p* spectra both from the fresh surface and the same surface after 20 min of sputtering. The S 2*p* line before sputtering is slightly skewed toward higher binding energy. This is the result of the S $2p_{3/2,1/2}$ spin-orbit splitting, which is unresolvable at the energy resolution of nonmonochromatic XPS. However, sputtering produces a shoulder centered approximately 2 eV below the main S 2*p* line.

Discussion

Quartz

The physical and chemical effects of ion bombardment on quartz and amorphous silica (bulk and thin film) have been extensively studied because of their use in electrical and optical devices (Burman and Landford, 1983; Hofmann and Thomas, 1983; Fischer et al., 1983, and references therein; Ajioka and Ushio, 1986). Hofmann and Thomas (1983) and Ajioka and Ushio (1986) have shown that for thin films of amorphous SiO_2, the Si and O photoelectron lines broaden with ion bombardment, but that the composition of the surface remains unchanged. This is essentially what we see for quartz, although there is an 11% reduction in the O/Si atomic ratio during the first

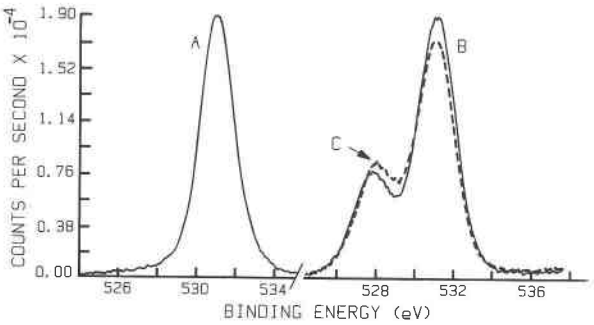

Fig. 3. Calcite O 1*s* spectra before sputtering (A), after 20 min of sputtering with the sample at 0° tilt during data collection (B), and after 20 min of sputtering with the sample at 65° tilt during data collection (C). The intensity scale refers to spectra B and C. Peak A has been scaled down from a full scale of 2.3 × 10^4 counts per second for easier comparison.

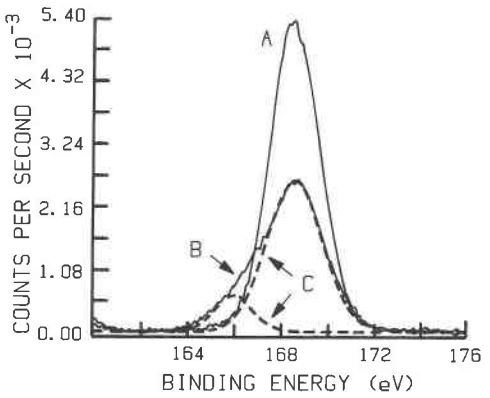

Fig. 4. Anhydrite S 2*p* spectra before sputtering (A) and after 20 min of sputtering (B). Curves labeled C are Gaussian-Lorentzian curves that sum to spectrum B and represent S^{6+} (168.5 eV) and S^{4+} (166.0 eV).

minute of sputtering. After this, the O/Si ratio remains nearly constant for the remainder of the experiment, showing only a net 1% rise during the next 19 min of sputtering (Fig. 1a). This compositional variation during the first minute of sputtering could have two explanations. First, O could initially have a higher sputtering rate compared to Si, after which the two could have comparable sputtering rates. This case involves a phenomenon known as *preferential* or *differential sputtering,* which occurs when the sputtering yields of two or more elements in the same material significantly differ. This phenomenon has been documented in a number of cases (e.g., see the review by Pivin, 1983). In a material consisting of two elements, as the element that is preferentially sputtered is selectively depleted from the near-surface region, its sputtering rate is reduced until it matches that of the more slowly sputtered element. Therefore, as the material is sputtered away, a depletion front advances through the material ahead of the retreating surface and the sputtering of both components remains in a steady state. If this scenario were true for quartz, and O initially sputtered preferentially relative to Si as suggested by Figure 1a, it follows that charge reduction of near-surface Si would be required. In fact, the reduction of metal oxides by ion bombardment has been documented in a large number of cases (Storp, 1985, and references therein). However, the Si^0 photoelectron peak has a chemical shift of 4 eV relative to the Si^{4+} 2*p* peak (e.g., Grunthaner et al., 1987), and there is no indication of any reduced Si in any of the Si 2*p* spectra collected for quartz in this study. It is possible that quartz could be reduced by sputtering under much higher beam-current densities than used in this study.

A second possibility that could explain the compositional trend shown in Figure 1a involves O-containing surface contamination. As stated earlier, the fractured surfaces analyzed in these experiments were briefly exposed to air. Fractured surfaces are highly reactive, and monolayer contamination is known to form instantaneously on most fresh mineral surfaces in air (e.g., see Hochella et al., 1986a). Therefore, the initial slight reduction of the O/Si ratio may instead be due to the removal of monolayer to submonolayer quantities of O-containing contaminants (probably dissociated O_2 or H_2O molecules since no C was observed in the initial survey scan). Complete removal of this contamination layer would easily take place in the first minute considering the surface removal rate for the beam conditions used (approximately 0.7 nm/min). Because Si^0 is not detected on the quartz surface, surface contamination is the most likely explanation for the apparent compositional change during the first minute of sputtering.

The broadening O 1*s* and Si 2*p* photoelectron peaks for quartz with ion bombardment suggest that both O and Si are influenced by a wider-than-normal range of atomic environments due to sputtering. Justification for interpreting the O 1*s* line in this way can be found in Hochella and Brown (1988). They have shown that the width of the O 1*s* line can be used as a measure of the number of unique oxygen-bonding environments in a structure. In this case, the bonding environment is defined as the number and type of ligands around the O, but does not include variations in site geometry. Although this observation is valid for the 12 silicates (including quartz) tested in Hochella and Brown (1988), the chemical shift of the O 1*s* line for different structural environments is quite variable, and the width of the O 1*s* line will not always be directly proportional to the number of O-bonding environments in all silicates. However, an increase in the width or change in the form of the O 1*s* line shape invariably indicates an increase in the number of O environments. For quartz, the width of the O 1*s* line increases rapidly during the first minute of sputtering and thereafter increases more slowly. Because it is most likely that the near-surface composition of quartz remains stoichiometric as discussed above, the increase in O-bonding environments is probably due to implanted Ar and defects created by the incoming ions. The creation

of structural defects in the near-surface region due to ion bombardment is well-known from TEM studies (e.g., see Barber, 1970; Goodhew, 1972). In addition, although it is clear that the near-surfaces of most crystalline materials become amorphous due to ion bombardment (Naguib and Kelly, 1975, and references therein; Veblen, 1985; Howitt, 1986), it is important to remember that this in itself will not result in broader photoelectron peaks, as shown by Hochella and Brown (1988).

Albite

Braun et al. (1977) used AES in an attempt to track near-surface compositional changes in albite due to sputtering. However, high electron-current densities were used to collect the Auger spectra. It is known that electron beams can cause significant changes in feldspar near-surface composition even at relatively low current densities (Hochella et al., 1986a). Therefore, the changes seen for albite by Braun et al. (1977) are most likely due to *both* ion and electron bombardment.

There are major changes in the near-surface composition of albite during the first 3 to 4 min of sputtering (Fig. 1b). After this time, the change in near-surface composition with continued sputtering is considerably smaller, and allowing for the estimated error in $\Delta\%$, an apparent steady state has been reached. As mentioned previously, this result has been duplicated by sputtering another albite sample for a total of 30 min. Again, after 4 min, all ratios had reached an apparent steady state.

Considering the relative trends of all six elemental ratios, the element that sputters most rapidly is Na, followed by Si, O, and Al. Therefore, depleted surface layers of Na (with respect to Al, O, and Si), Si (with respect to O and Al), and O (with respect to Al) develop during the first 3 to 4 min, eventually equalizing the relative sputtering probabilities of all four constituent elements. Continued sputtering simply moves these depleted fronts into the crystal as the surface is eroded away.

It should be noted that the initial survey spectrum of the albite surface showed the presence of a small amount of adventitious C, most likely due to CO_2 attachment during the brief exposure to air before insertion into the instrument. However, the C line was not present in the survey spectrum taken after 1 min of sputtering. Therefore, the shapes of the atomic ratio curves (Fig. 1b) should not be affected by adventitious elements after this time.

The high-resolution spectra collected for albite show that the widths of the O 1*s*, Al 2*p*, and Si 2*p* photoelectron lines, along with the Na *KLL* Auger line, all increase significantly during the initial stages of sputtering. As shown in Figure 2, the width of the O 1*s* line shows an increase after the first minute of sputtering and thereafter remains essentially constant. The other three lines reach maximum width after no more than 3 min of sputtering (not shown). As with quartz, none of the peaks suggests the presence of a new resolvable component, but instead only shows an increase in width. The O 1*s* line can be interpreted as undergoing a width increase, like quartz, because of the implantation of Ar and the creation of defects, but also because preferential sputtering should result in additional O-bonding environments in the near-surface region. Although not specifically demonstrated for Na, Al, and Si lines as with O, similar arguments for line broadening should be appropriate for these elements.

Calcite

The near-surface composition of calcite, like albite, changes quickly during the first 3 to 4 min of ion bombardment and thereafter remains relatively stable to the end of the experiment. However, the compositional changes with calcite are more pronounced than those for albite; the Ca/C ratio more than doubles in just 3 min of sputtering (Fig. 1c). Further, the relative positions of the atomic ratio trends plotted in Figure 1c indicate that C sputters most rapidly from calcite under these conditions, followed by O and Ca.

During sputtering, the Ca 2*p* and the C 1*s* lines become broader, but otherwise do not show a shape change, and no new peaks appear. This is not the case for the O 1*s* line, as a new O line appears after just 1 min of sputtering (Figs. 2 and 3). As sputtering continues, the new O 1*s* photoelectron peak continues to grow in intensity and broaden; the original O 1*s* line broadens considerably over the first 3 min before its width stabilizes (Fig. 2).

The order of preferential sputtering is consistent with a simple $CaCO_3 \rightarrow CaO + CO_2$ breakdown reaction. However, the position of the new O 1*s* line (528.3 eV) does not correspond with the position of the O 1*s* line in pure CaO (530.8 eV) recently measured in our laboratory. Although the new material created by the ion bombardment has not been identified, it is clear that it is, on the average, on the surface overlying the calcite. This has been confirmed with angle-resolved XPS. Figure 3 shows the difference between data collected on the ion-damaged surface at 0° and 65° tilt (the tilt angle is measured between the sample normal and the analyzer entrance axis; higher tilt angles result in a more surface-sensitive analysis). The new O 1*s* peak is enhanced and the calcite O 1*s* peak is diminished in the spectrum taken at 65° tilt.

Anhydrite

The effects of Ar-ion bombardment on anhydrite have been previously observed by Coyle et al. (1981) in an XPS study of several metal sulfates. They emphasized that the S 2*p* core level exhibits particularly large chemical shifts (e.g., Wagner et al., 1979), making S-containing compounds particularly interesting to study with photoelectron spectroscopy. Using Ar-ion bombardment at the same energy as this study (1 kV), but with beam-current densities in the milliampere range and ion doses up to 10^{18} ions/cm^2, their spectra show evidence for the generation of both partially and fully reduced S, as well as the preferential sputtering of S with respect to Ca.

Our spectra do not show evidence for fully reduced S (S^0 2*p* photoelectron line expected at approximately 162 eV), but the shoulder appearing to the low-binding-en-

ergy side of the S 2*p* peak after sputtering (Fig. 4) definitely indicates a reduction of some near-surface S from S^{6+} to S^{4+} and suggests the presence of $CaSO_3$. Gaussian-Lorentzian curves fit to this S 2*p* peak (Fig. 4) show that the chemical shift between these two S oxidation states is approximately 2.5 eV. Lindberg et al. (1970) documented a similar chemical shift (2.2 eV) for the S 2*p* peak from $Na_2S^{6+}O_4$ and $Na_2S^{4+}O_3$.

As mentioned previously, the change in the anhydrite near-surface composition as a result of sputtering is dramatic, especially considering the Ca/S ratio that more than doubles after just 3 min of sputtering (Fig. 1d). It is also interesting to note that S sputters preferentially relative to O. In apparent agreement with this, Coyle et al. (1981) observed that for sulfates containing metals that form very stable oxides, continued sputtering resulted in the complete loss of S and the formation of an oxide in the near-surface region. Therefore, in the case of anhydrite, it is likely that sputtering produces CaO as well as the previously mentioned calcium sulfite. The shoulder that appears on the O 1*s* line of anhydrite after sputtering (528.1 eV) is at approximately the same binding energy as the shoulder of the O 1*s* line of sputtered calcite (528.3 eV), adding further evidence for the presence of a simple oxide phase.

Summary and conclusions

1. Quartz, albite, calcite, and anhydrite were bombarded with 45° incident 1-kV Ar ions for a total of 20 min each (10^{17} ions/cm^2). Under these conditions, it has been estimated that each mineral has undergone between 10 and 20 nm of surface removal. Each target showed evidence of near-surface structural change, and albite, calcite, and anhydrite underwent significant compositional modifications due to relative preferential sputtering trends as follows: albite, Na > Si > O > Al; calcite, C > O > Ca; anhydrite, S > O > Ca. Quartz did not show direct evidence of preferential sputtering under these conditions.

2. Significant structural and compositional changes can occur within the first minute of sputtering under the conditions used in this study. The most dramatic examples of compositional change occurred with calcite and anhydrite. The Ca/C and Ca/S concentration ratios in the near-surface region of calcite and anhydrite, respectively, more than double in the first minute of sputtering. In addition, because O is known to preferentially sputter with respect to cations in a number of oxides (Yin et al., 1976; Brundle et al., 1977; Storp and Holm, 1979; Storp, 1985; this study), it is surprising to note that Si sputters preferentially to O in albite, both of which sputter preferentially with respect to Al. This suggests that an aluminum oxide is the most sputter-resistant compound in the ion-damaged near-surface of albite.

Structural changes were indicated by changes in the width of photoelectron peaks, or the appearance of shoulders or fully resolved new lines. Structural changes result from the physical implantation of Ar, the creation of defects, compositional changes due to preferential sputtering, and the mixing of near-surface layers. As a result, the near-surfaces of most minerals become amorphous during ion bombardment at energies commonly used (0.5 to 5.0 kV) for sputter depth profiling.

3. Considering measurement error, most of the atomic ratio curves (Figs. 1a–1d) and the O 1*s* FWHM curves (Fig. 2) seem to be approaching a near-steady state after only 3 to 4 min of sputtering. This corresponds to a surface removal of approximately 2–3 nm, which is also roughly the maximum depth of penetration of the incoming ions. This apparent relationship between the maximum depth of penetration and the time needed before steady state is reached has been noted before for binary alloys (Pivin, 1983, and references therein). Significant changes in the atomic ratio curves after the time needed to reach steady state should indicate a true compositional gradient inherent to the sample and not the sputter process. Where compositional changes are anticipated in the top several nanometers, it is recommended that a sputter profile into a standard homogeneous sample similar to the unknown be performed first to provide a baseline profile.

4. Sputter depth profiling is generally used for compositional information, but XPS also provides oxidation and/or structural-state information. Therefore, for example, sputter depth profiling with XPS could be used to determine the distribution of Fe oxidation states in the near-surface regions of important Fe-containing minerals. The near-surfaces of Fe-containing silicates have been shown to directly influence the redox chemistry of species in aqueous solution in contact with these surfaces (White and Yee, 1985). Unfortunately, such oxidation-state profiling cannot generally be performed on minerals due to preferential sputtering.

5. Although the use of implanted Ar as a charge-reference standard in insulators is theoretically sound (Kohiki et al., 1983a, 1983b), its practical use for minerals is limited owing to the significant structural damage and compositional changes that can be encountered during the implanting process. In this study, in order to implant enough Ar into the quartz, albite, calcite, and anhydrite near-surfaces such that the Ar 2*p* line position could be accurately measured, between 1 and 6 min of sputtering at 1 kV was necessary. With significant changes to the near-surface occurring in this time frame, the usefulness of this charge-reference technique is greatly reduced.

Acknowledgments

This work was generously supported by the USGS, the National Science Foundation through Stanford's Center for Materials Research, and the Chevron Oil Field Research Company. Comments on the original manuscript from Richard J. Reeder and David R. Veblen and two anonymous reviewers were greatly appreciated.

References cited

Ajioka, T., and Ushio, S. (1986) Characterization of the implantation damage in SiO_2 with X-ray photoelectron spectroscopy. Applied Physics Letters, 48, 1398–1399.

Bancroft, G.M., Brown, J.R., and Fyfe, W.S. (1977) Calibration studies for quantitative ESCA of ions. Analytical Chemistry, 49, 1044–1048.

Barber, D.J. (1970) Thin foils of non-metals made for electron microscopy by sputter-etching. Journal of Materials Science, 5, 1–8.

Berner, R.A., and Holdren, G.H., Jr. (1977) Mechanism of feldspar weathering: Some observational evidence. Geology, 5, 369–372.

——— (1979) Mechanism of feldspar weathering. II. Observations of feldspars from soils. Geochimica et Cosmochimica Acta, 43, 1173–1186.

Braun, P., Farber, W., Betz, G., and Viehbock, F.P. (1977) Effects in Auger electron spectroscopy due to the probing electrons and sputtering. Vacuum, 27, 103–108.

Brule, D.G., Brown, J.R., Bancroft, G.M., and Fyfe, W.S. (1980) Cation adsorption by hydrous manganese dioxide: A semi-quantitative X-ray photoelectron spectroscopic (ESCA) study. Chemical Geology, 28, 331–339.

Brundle, C.R., Chuang, T.J., and Wandelt, K. (1977) Core and valence level photoemission studies of iron oxide surfaces and the oxidation of iron. Surface Science, 68, 459–468.

Burman, C., and Lanford, W.A. (1983) Radiation damage enhancement of the penetration of water into silica glass. Journal of Applied Physics, 54, 2312–2315.

Carter, G., and Colligon, J.S. (1968) Ion bombardment of solids, 446 p. Elsevier, New York.

Coyle, G.J., Tsang, T., Adler, I., and Ben-Zvi, N. (1981) XPS studies of ion-bombardment damage of transition metal sulfates. Journal of Electron Spectroscopy and Related Phenomena, 24, 221–236.

Dillard, J.G., Crowther, D.L., and Murray, J.W. (1982) The oxidation states of cobalt and selected metals in Pacific ferromanganese nodules. Geochimica et Cosmochimica Acta, 46, 755–759.

Fischer, H., Gotz, G., and Karge, H. (1983) Radiation damage in ion-implanted quartz crystals. II. Annealing behaviour. Physica Status Solidi, 76, 493–498.

Fung, P.C., Bird, G.W., McIntyre, N.S., Sanipelli, G.G., and Lopata, V.J. (1980) Aspects of feldspar dissolution. Nuclear Technology, 51, 188–196.

Goodhew, P.J. (1972) Specimen preparation in materials science, 180 p. North-Holland, Amsterdam.

Grunthaner, P.J., Hecht, M.H., Grunthaner, F.J., and Johnson, N.M. (1987) The localization and crystallographic dependence of Si suboxide species at the SiO_2/Si interface. Journal of Applied Physics, 61, 629–638.

Hayes, K.F., Roe, A.L., Brown, G.E., Jr., Hodgson, K.O., Leckie, J.O., and Parks, G.A. (1987) In situ X-ray adsorption study of surface complexes: Selenium oxyanions on α-FeOOH. Science, 238, 783–786.

Hochella, M.F., Jr. (1988) Auger electron and X-ray photoelectron spectroscopies. Mineralogical Society of America Reviews in Mineralogy, 18, 573–637.

Hochella, M.F., Jr., and Brown, G.E., Jr. (1988) Aspects of silicate surface structure analysis using X-ray photoelectron spectroscopy (XPS). Geochimica et Cosmochimica Acta, 52, 1641–1648.

Hochella, M.F., Jr., and Carim, A.H. (1988) A reassessment of electron escape depths in silicon and thermally grown silicon dioxide thin films. Surface Science, 197, L260–L268.

Hochella, M.F., Jr., Harris, D.W., and Turner, A.M. (1986a) Scanning Auger microscopy as a high-resolution microprobe for geologic materials. American Mineralogist, 71, 1247–1257.

——— (1986b) High resolution scanning Auger microscopy of mineral surfaces. Scanning Electron Microscopy, 1986, 337–349.

Hochella, M.F., Jr., Ponader, H.B., Turner, A.M., and Harris, D.W. (1988) The complexity of mineral dissolution as viewed by high resolution scanning Auger microscopy: Labradorite under hydrothermal conditions. Geochimica et Cosmochimica Acta, 52, 385–394.

Hofmann, S. (1980) Quantitative depth profiling in surface analysis: A review. Surface and Interface Analysis, 2, 148–160.

Hofmann, S., and Thomas, J.H., III. (1983) An XPS study of the influence of ion sputtering on bonding in thermally grown silicon dioxide. Journal of Vacuum Science and Technology B, 1, 43–47.

Holdren, G.R., Jr., and Berner, R.A. (1979) Mechanism of feldspar weathering—I. Experimental studies. Geochimica et Cosmochimica Acta, 43, 1161–1171.

Howitt, D.G. (1986) Radiation effects encountered by inorganic materials in analytical electron microscopy. In D.C. Joy, A.D. Romig, Jr., and J.I. Goldstein, Eds., Principles of analytical electron microscopy, p. 375–392. Plenum, New York.

Kohiki, S., Ohmura, T., and Kusao, K. (1983a) A new charge-correction method in X-ray photoelectron spectroscopy. Journal of Electron Spectroscopy and Related Phenomena, 28, 229–237.

——— (1983b) Appraisal of a new charge correction method in X-ray photoelectron spectroscopy. Journal of Electron Spectroscopy and Related Phenomena, 31, 85–90.

Lindberg, B., Hamrin, K., Johansson, G., Gelius, U., Fahlmann, A., Nordling, C., and Siegbahn, K. (1970) Valence bands and core levels of the isoelectronic series LiF, BeO, BN, and graphite studied by ESCA. Physica Scripta, 1, 277–280.

Mucci, A., and Morse, J.W. (1985) Auger spectroscopy determination of the surface-most adsorbed layer composition on aragonite, calcite, dolomite, and magnesite in synthetic seawater. American Journal of Science, 285, 306–317.

Mucci, A., Morse, J.W., and Kaminsky, M.S. (1985) Auger spectroscopy analysis of magnesian calcite overgrowths precipitated from seawater and solutions of similar composition. American Journal of Science, 285, 289–305.

Murray, J.W., and Dillard, J.G. (1979) The oxidation of cobalt(II) adsorbed on manganese dioxide. Geochimica et Cosmochimica Acta, 43, 781–787.

Myhra, S., White, T.J., Kesson, S.E., and Riviere, J.C. (1988) X-ray photoelectron spectroscopy for the direct identification of Ti valence in $[Ba_xCs_y][(Ti,Al)^{3+}_{2x+y}Ti^{4+}_{8-2x-y}]O_{16}$ hollandites. American Mineralogist, 73, 161–167.

Naguib, H.M., and Kelly, R. (1975) Criteria for bombardment-induced structural changes in non-metallic solids. Radiation Effects, 25, 1–12.

Penn, D.R. (1987) Electron mean-free-path calculations using a model dielectric function. Physical Review B, 35, 482–486.

Perry, D.L., Tsao, L., and Gaugler, K.A. (1983) Surface study of HF- and HF/H_2SO_4-treated feldspar using Auger electron spectroscopy. Geochimica et Cosmochimica Acta, 47, 1289–1291.

Perry, D.L., Tsao, L., and Taylor, J.A. (1984) The galena/dichromate solution interaction and the nature of the resulting chromium(III) species. Inorganica Chimica Acta, 85, L57–L60.

Petit, J.-C., Mea, G.D., Dran, J.-C., Schott, J., and Berner, R.A. (1987) Mechanism of diopside dissolution from hydrogen depth profiling. Nature, 325, 705–707.

Petrovic, R., Berner, R.A., and Goldhaber, M.B. (1976) Rate control in dissolution of alkali feldspar—I. Study of residual feldspar grains by X-ray photoelectron spectroscopy. Geochimica et Cosmochimica Acta, 40, 537–548.

Pivin, J.C. (1983) An overview of ion sputtering physics and practical implications. Journal of Materials Science, 18, 1267–1290.

Powell, C.J. (1984) Inelastic mean free paths and attenuation lengths of low-energy electrons in solids. Scanning Electron Microscopy, 1984, 1649–1664.

Schott, J., Berner, R.A., and Sjoberg, E.L. (1981) Mechanism of pyroxene and amphibole weathering. I. Experimental studies of iron-free minerals. Geochimica et Cosmochimica Acta, 45, 2123–2135.

Seah, M.P., and Dench, W.A. (1979) Quantitative electron spectroscopy of surfaces: A standard data base for electron inelastic mean free paths in solids. Surface and Interface Analysis, 1, 2–11.

Storp, S. (1985) Radiation damage during surface analysis. Spectrochimica Acta, 40B, 745–756.

Storp, S., and Holm, R. (1977) ESCA investigations of ion beam effects on surfaces. Surface Science, 68, 459–468.

Thomassin, J.H., Goni, J., Baillif, P., Touray, J.C., and Jaurand, M.C. (1977) An XPS study of the dissolution kinetics of chrysotile in 0.1 *N* oxalic acid at different temperatures. Physics and Chemistry of Minerals, 1, 385–398.

Tsang, T., Coyle, G.J., and Adler, I. (1979) XPS studies of ion bombardment damage of iron-sulfur compounds. Journal of Electron Spectroscopy and Related Phenomena, 16, 389–396.

Veblen, D.R. (1985) High-resolution transmission electron microscopy. In J.C. White, Ed., Short course in applications of electron microscopy in the earth sciences, p. 63–90. Mineralogical Association of Canada, Toronto.

Wagner, C.D., Riggs, W.M., Davis, L.E., Moulder, J.F., and Muilenberg, G.E. (1979) Handbook of X-ray photoelectron spectroscopy, 190 p. Physical Electronics, Eden Prairie, Minnesota.

White, A.F., and Yee, A. (1985) Aqueous oxidation-reduction kinetics associated with coupled electron-cation transfer from iron-containing silicates at 25 °C. Geochimica et Cosmochimica Acta, 49, 1263–1275.

Yin, L., Ghose, S., and Adler, I. (1972) Investigation of a possible solar-wind darkening of the lunar surface by photoelectron spectroscopy. Journal of Geophysical Research, 77, 1360–1367.

Yin, L., Tsang, T., and Adler, I. (1976) On the ion-bombardment reduction mechanism. Proceedings of the Lunar Science Conference, 7, 891–900.

Manuscript received February 29, 1988
Manuscript accepted July 29, 1988